Improvement of rejection band with Defected Microstrip Line and Ground plane Resonators

Somdotta Roy Choudhury

Department of Electronics & Telecommunication Engg., Ramrao Adik Institute of Technology, D. Y. Patil Deemed to be university, Navi Mumbai, Maharashtra- 400706, India

Corresponding author: Somdotta Roy Choudhury (e-mail: somdottaroychoudhury@mail.com).

ABSTRACT In this paper a unique spiral defected microstrip line structure is studied, simulated and measured. This proposed resonating structure provides a dual band bandstop filter response for Wi-Fi communication and remote sensing applications. Next proposed spiral defect is combined with the hexagonal head defected resonators at ground plane to improve the rejection band. In addition a study is also done to observe the effects of the proposed defects at both signal plane and ground plane. A comparison is done among the response of individual defects filters and combined defect filter. It is observed that later shows improved overall bandwidth with compactness. The proposed combined defect filter with improved stopband displays 92.6% FBW and 112.5 dB/GHz sharpness factor with very compact in size as $0.26 \lambda_0 \times 0.25 \lambda_0$. All measurement results are in good agreement with the simulated results.

INDEX TERMS Bandstop filter, microstrip line, hexagonal head DGS, spiral slot DMS, wide band.

I. INTRODUCTION

IN modern days' satellite and mobile communication system require high performance microstrip circuits with compact size and low cost. Thus progressive research works are carried out to get better performance of the Improving microstrip technology. the characteristics is very needful to suppress the spurious signals from transmitters, mixers, power amplifiers, and so on. Various techniques are adopted such as open stubs, stepped impedance resonators and different defected structures. Some defects are in the ground plane under microstrip line and some are the defect in the signal plane of microstrip line. The defected structures in ground plane called Defected Ground Structure (DGS) which effectively disturb shield current distribution in ground plane [1]. The defects are generally in the form of slots with single or periodic geometric structures which yields band rejection responses [2]. In [3] stepped-impedance DGS with a folded slot at ground generates dual resonance. An open loop defected ground structure [4] is created to increase coupling as well as transmission zeros in an ultra-broad band filter. A square DGS used to increase the mode characteristic impedance of parallel couple line by decreasing the shunt capacitance effect between the microstrip lines and the ground in [5] and resulting in stepped-impedance resonator. A tunable substrate integrated defected ground structure is introduced in [6] which is an combination of DGS and substrate integrated waveguide (SIW), to provide higher inductance but lower characteristic impedance, leading to wider stop band. Defected Microstrip Structure (DMS) on the other hand, is a defected structure on the signal plane of the microstrip line. These structures also gives stop band response without increasing the filter size. In [7] a spiral geometry DMS is introduced to provide the narrow rejection band and reduced size. A DMS is created on a stub loaded stepped impedance resonator to generate a tri band and guad band bandpass response [8, 9]. An ultrawideband bandpass filter is designed using a T-shaped resonator in [10] with dual notch bands which is achieved by "L"-shaped DMS. An analytical design method is proposed to present spiral DMS and validated by experimental fabrication in [11]. Another a stub-loaded stepped-impedance resonator with DMS is proposed in [12] to design a quad band bandpass filter for GPS, WiFi, WLAN, and WiMAX applications. The concept of DMS used in [13] to design a dual-band bandstop filtering cable by using asymmetric bridge-connected spiral-shaped defect. In [14] a "T" shaped top plane defect or DMS is combined with dumbbell shaped ground plane defect or DGS to build an improved response lowpass filter. A multilayered WLAN band bandpass filter is designed using U-shaped DGS resonators and T shaped DMS in [15]. Again a different "T" shaped DMS and U-shaped DGS are employed to make a miniaturized dual-band bandstop filter [16]. An interdigital-DGS-DMS lowpass filter is achieved using two cascaded "T" shaped DMS, one interdigital shaped DMS and rectangular DGS slots in [17]. A wide stopband lowpass filtering response is achieved using coupled stub-loaded resonators with "T" shaped DMS resonators and dumbbell DGS structures [18]. Another



lowpass filter is proposed for RADAR and GPS application by using quasi octagonal stub resonators, two DMSs and arrowhead DGS in [19]. One SIW Bandpass filter is investigated in [20] with inclusion of DGS and DMS structures. In [21] an X-band bandstop filter is proposed by using DGS and DMS combined structures.

Here in this paper, a spiral signal plane defected resonator is introduced, analysed and measured. This proposed spiral resonator is then combined with the hexagon head defected structures at ground plane to provide wide band lowpass filter response. The initial work depicted in section II, introduced, analyzed and measured a spiral shape defected Microstrip line resonator. In section-III, a study of the spiral defect at signal plane combined with hexagonal headed defected structures at ground plane is performed which yields an improved rejection band lowpass filter. In section IV, a study of comparative analysis of combined structures with the individual ones is presented. Another comparative analysis is also given for the proposed filter with the available literature.

II. ANALYSIS OF SPIRAL MICROSTRIP LINE DEFECTED STRUCTURE

A. GEOMETRY OF SPIRAL SHAPED DEFECT RESONATOR

Spiral defects is a rectangular folded slot etched on the microstrip line. This defect starts at the edge of the signal line and then folds in a certain manner to provide a spiral shape. Fig. 1 shows the schematic diagram of the defect unit consisting of spiral shaped slot etched off the microstrip line. The substrate with a dielectric constant of 4.4 and thickness of 1.59 mm is considered for the microstrip line. The width (W) of the microstrip line is obtained as 3 mm corresponding to 50-Ohm characteristics impedance. The different dimensions of spiral shaped defect have been taken as a1= 3.7 mm, a2= 2.5 mm, a3= 2.5 mm, b1=0.4mm, b2= 0.3 mm, b3= 2.2mm, b4=1.6mm, g= 0.3 mm. The total cut out size of proposed defect unit is (4.35 X 2.6) mm².

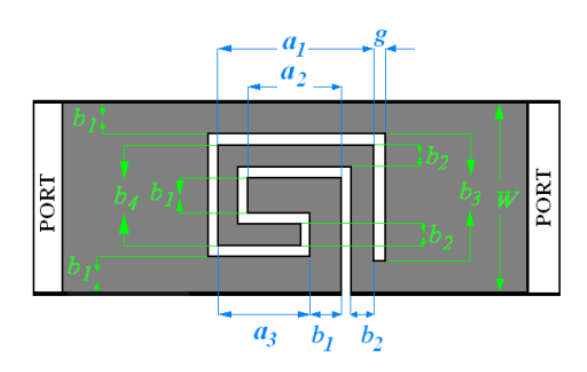
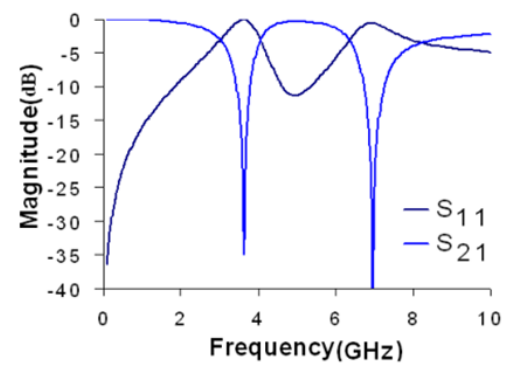


FIGURE 1. Schematic diagram of the spiral defect unit.

B. SIMULATED RESULTS

From the MoM (IE3D simulation software) based simulated S-parameters as shown in Fig. 2, it is observed that the investigated defect unit provides dual stopband response with centre frequencies at 3.6GHz and 6.9 GHz. The lower and upper cutoff frequencies of the first band are 3.03 GHz and 4.06 GHz while those of the second stopband are at 6.36 GHz and 8.57 GHz. The attenuation levels of the first and second rejection bands are of 34.7 dB and 44.5 dB respectively. The passband insertion loss is of 0.4dB. The 20 bandwidth of the first band is 104MHz while that is of 154 MHz for the second band. The sharpness factors observed at the lower and upper edge of the passband are 51.78 dB/GHz and 75.2 dB/GHz respectively for the first band and those for the second stopband are 69 dB/GHz and 25.9 dB/GHz



respectively.

FIGURE 2. Simulated s-parameters of the spiral defect unit.

C. EQUIVALENT CIRCUIT

This proposed spiral DEFECT unit produces two-pole Butterworth bandstop filter response which is described by two LC parallel resonant circuit connected in series with 50 Ohm transmission line on both ends as shown in Fig. 3. For the given dimension of the proposed structure the extracted inductances are given by: L1=1.24 nH and L2=491.4 pH whereas capacitances are: C1 =1.54 pF and C2=1.06pF. Corresponding circuit simulation response is compared with the simulated response and illustrated in Fig. 4.

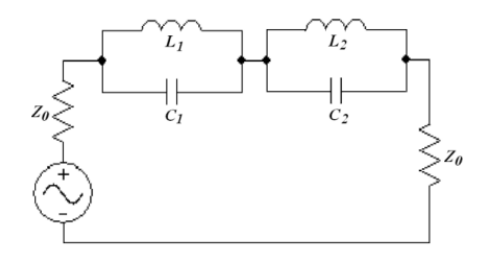


FIGURE 3. Equivalent circuit model of the proposed spiral defect.

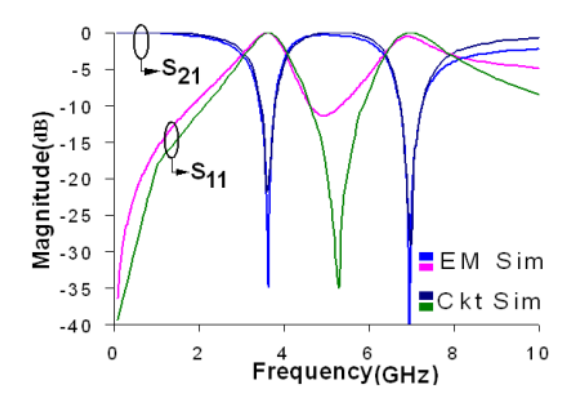


FIGURE 4. Comparison of the EM simulated and circuit simulated response.

D. TRANSMISSION LINE MODEL

The operation of the proposed spiral defected structure can be understood well by the transmission line model equivalence, which is shown by Fig. 5 (a) and Fig.5 (b) for the two stopbands respectively. This equivalent circuit model is obtained by dividing the line into three parts: one transmission lines (through lines) at the top of the spiral defect having characteristic impedance Z_1 and the electrical length θ_1 , two resonating stub line having characteristic impedances Z_2 and Z_1 and electrical lengths θ_2 and θ_3 respectively These two stubs (Z_2 , θ_2 and Z_1 , θ_3) [3, 24, 25] are open circuited and quarter wavelength long corresponding to the two resonant frequencies f_1 and f_2 . The through line is half wavelength long and the input impedances looking at the left side of the two stubs are given by,

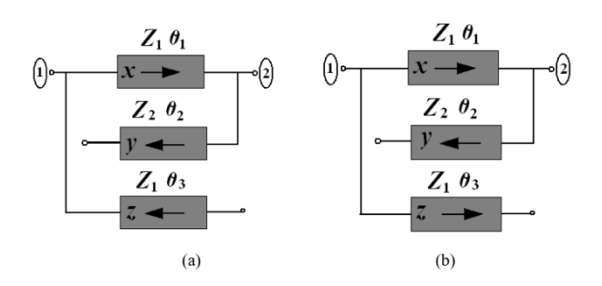


FIGURE 5. (a) Transmission line model equivalent model of the proposed defect for the first resonant frequency, (b) Transmission line model equivalent model of the proposed defect for the second resonant frequency.

$$Z_{in1} = Z_{stub1} \| Z_{through} \tag{1}$$

$$Z_{in2} = Z_{stub2} \| Z_{through}$$
 (2)

Where, Z_{stub1} and Z_{stub2} are the input impedances looking into the first stub having characteristic impedance Z_2 and the second stub having characteristic impedance Z_1 respectively. The $Z_{through}$ is the input impedance looking into the through line. The input impedances Z_{stub1} and Z_{stub2} are given by equations (3) and (4) respectively.

$$Z_{stub1} = -jZ_2 \cot \theta_2 \tag{3}$$

$$Z_{stub2} = -jZ_1 \cot \theta_3 \tag{4}$$

Since the through line is half wavelength long it repeat itself at the start of the second stub. For the stub length $(\theta=\beta l)$ of quarter wavelength long the Zin1 and Zin2 becomes zero and the signal reflected back to the source and causes transmission zeros to be occurred. The corresponding transmission coefficient and reflection coefficient are illustrated in equations (5) and (6) given below [24].

$$S_{11} = \frac{A+B/Z_0 - CZ_0 - D}{A+B/Z_0 + CZ_0 + D}$$
 (5)

$$S_{21} = \frac{2}{A+B/Z_{-}+CZ_{-}+D}$$
 (6)

Where,

$$\begin{split} A &= A_X A_Y A_Z \\ B &= B_X B_Y B_Z \\ C &= C_X C_Y C_Z \text{ and } D = D_X D_Y D_Z \end{split}$$

In which the ABCD parameters are:

$$\begin{array}{ll} A_X = \cos\theta_1 & B_X = jZ_1\sin\theta_1 \\ C_X = jY_1\sin\theta_1 & D_X = \cos\theta_1 \\ A_Y = 1 & B_Y = 0 \\ C_Y = j\tan\theta_2/Z_2 & D_Y = 1 \\ A_Z = \cos\theta_3 & B_Z = jZ_1\sin\theta_3 \\ C_Z = jY_1\sin\theta_3 & D_Z = \cos\theta_3 \end{array}$$

E. SURFACE CURRENT DISTRIBUTION

The surface current distributions for the two resonant frequencies are given in Fig. 6 (a) and Fig. 6 (b). From the Fig. 5 (a), (b) and Fig. 6 (a), (b), it is obvious that for the first

resonance the stub 1 or the transmission line section 'y' (characteristic impedance Z_2 and electrical length θ_2) draws maximum surface current while for the second resonance the stub 2 or the transmission line section 'z' (characteristic impedance Z_1 and electrical length θ_3).

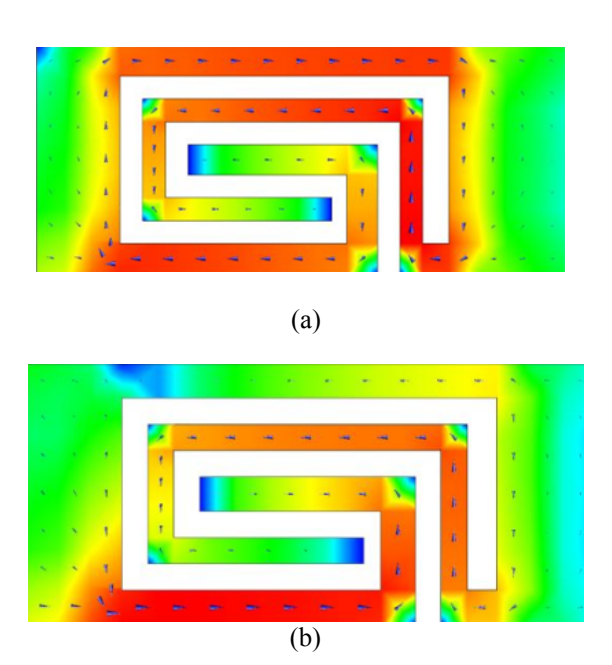


FIGURE 6. (a) Surface current distribution of the proposed defect for the first resonant frequency, (b) surface current distribution of the proposed defect for the second resonant frequency.

F. PARAMETRIC STUDY

The tuning of the resonant frequency can be done easily with the variation of the stub lengths 'y' and 'z' as illustrated in Fig. 5 and Fig.6. With the change of 'y' (y=A+B+C+D+E) and 'z' (z=M+N+P), the effective electric length, as well as inductance L, change proportionately, and the resonant frequency changes inversely, as shown in Fig. 7 (a). In this filter structure the arrangement of the circuit is such that if 'y' changes the 'z' also changes and vice versa hence in the Fig. 7 (a) and (b) only the change of resonant frequencies with 'y' is shown. The variation of attenuation pole and attenuation zero represented graphically in Fig. 7 (b). Following the Fig. 8, the expressions of the resonance frequencies of this proposed dual band bandstop filter using spiral shaped defect are depicted by following equations (7) and (8) [24].

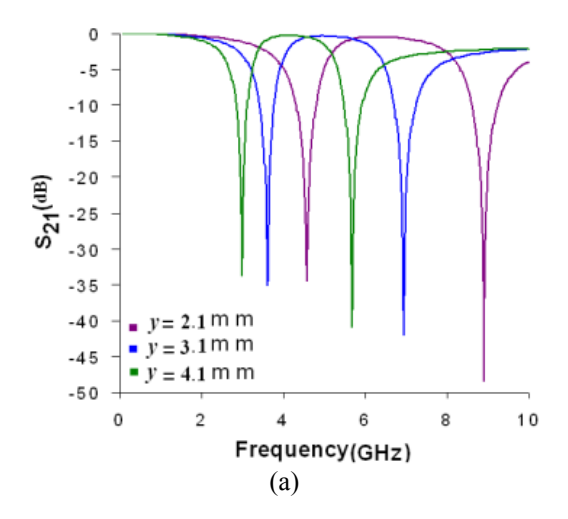
$$f_{r1} = \frac{\varepsilon}{4(A+B+C+D+E+F)/\varepsilon_{eff}}$$
(7)

$$f_{r2} = \frac{c}{4(M+N+P)\sqrt{\epsilon_{eff}}} \tag{8}$$

Where,

$$\varepsilon_{eff} = \frac{\varepsilon_r + 1}{2} + \frac{\varepsilon_r - 1}{2} \frac{1}{\sqrt{1 + 12 \frac{h}{w}}}$$

where c is the velocity of light in free space, ε_{eff} is the effective dielectric constant of the microstrip line, ε_r is the relative dielectric constant, w is the conductor strip width of the microstrip line and h is the substrate thickness.



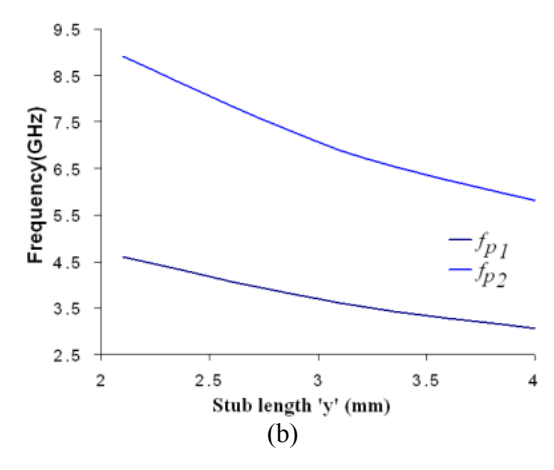


FIGURE 7. (a) Shows the variation of frequency with stubs having characteristic impedances Z_1 and Z_2 , (b) shows the variation of attenuation zero and attenuation pole frequency with stubs having characteristic impedances Z_1 and Z_2 .

TABLE I. Comparison between calculated resonant frequencies with the simulated ones.

l _I (mm)	<i>l</i> ₂ (mm)	f_{lcal} (GHz)	$f_{lsim}({ m GHz})$	$f_{2cal}(GHz)$	$f_{2sim}({ m GHz})$
13.9	8.8	3.1	3.0	4.9	5.6
12.0	6.8	3.61	3.61	6.4	6.9
10.0	4.8	4.3	4.5	9.0	8.9



Table 7 shows the comparison between calculated resonant frequencies with the simulated ones, where flcal and f2cal are the calculated resonant frequencies of the lower and higher band respectively and f1sim and f2sim are the simulated resonant frequencies of the lower and higher band respectively. Therefore by simply changing the effective stub lengths y (y=A+B+C+D+E) and z (z=M+N+P) the cutoff and pole frequencies of the filter for the both band can be changed, which is clearly shown by Fig. 7 (a) and (b).

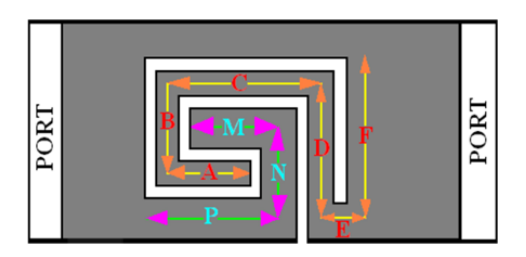


FIGURE 8. Schematic diagram showing the current directions in two stubs for two resonant frequencies.

G. MEASURED RESULT

The photographic view of this dual bandstop filter is shown in Fig. 9 (a). The comparison between the simulated and measured result of this 2-pole bandstop filter is given by Fig. 9 (b). It is clear from this figure that the simulated and the measured results are in good agreement. A minor dissimilarity occurs at higher frequencies may be due to fabrication error or SMA connetors. Fig. 9 (c) provides the measured phase response of the proposed structure.

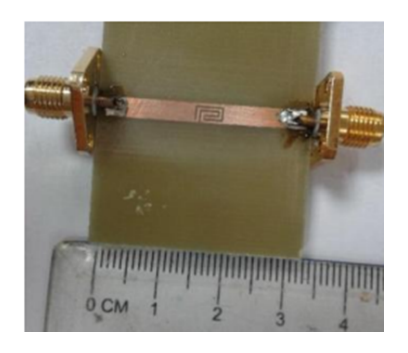


FIGURE 9. Photograph of the structure.

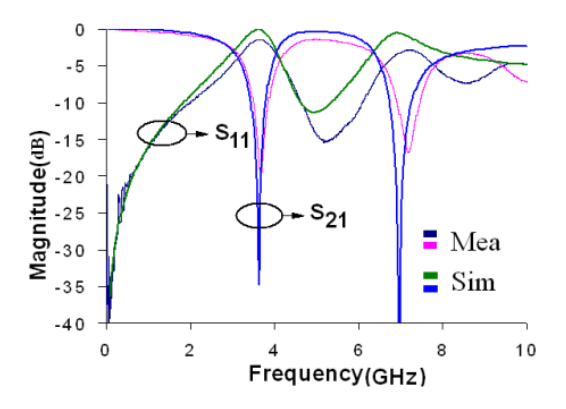


FIGURE 10. Comparison of simulated and measured S-parameter results.

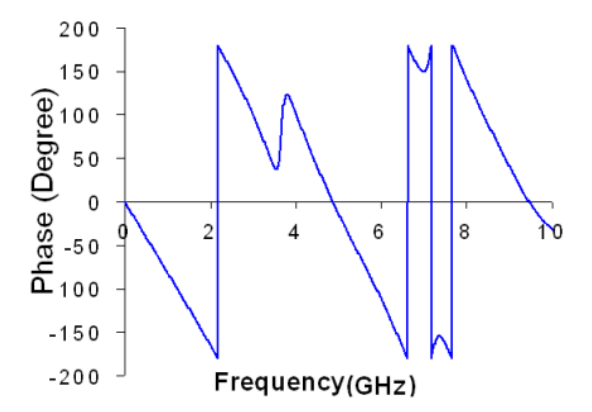


FIGURE 11. Measured phase response.

III. WIDE BAND BANDSTOP FILTER USING SPIRAL DEFECTS AND HEXAGONAL HEAD DEFECT

Here the proposed spiral shaped defect at microstrip line, introduced along with a dumbbell defect at the ground plane to improve the overall stopband by Stagger tuning action. Fig. 12(a) shows the schematic diagram of the proposed filter unit consisting of spiral shaped defected slot at the signal plane and a simple dumbbell shaped defect in the ground plane. The spiral shaped slot having an open end at the edge is etched off from the microstrip line. There is a small improvement in the microstrip line by means of high-low line, which is chosen here for impedance matching. The dumbbell shaped defect at ground is placed at both side of the spiral defect at top plane and exactly below the high-low microstrip line but at a distance of 11.4 mm at the ground plane. The substrate with a dielectric constant of 4.4 and thickness of 1.59 mm is considered for the filter design. The width (W2) of the microstrip line is obtained as 3 mm corresponding to 50-Ohm characteristics impedance. The different dimensions of spiral shaped defect have been taken as: a= 4 mm, b= 1.9 mm, 11=1.7mm, 12=1.7mm, 13=2.5mm, 14=2.6mm, 15=4.05mm, 16=0.45mm, h1=0.2mm, h2=0.1mm, h3=0.9mm, h4=0.9mm, h5=2mm, h6=2.1mm, W1=10mm, W2=3mm, W3=10 mm, g1=0.2mm, g2=0.2mm, L=11.4mm.

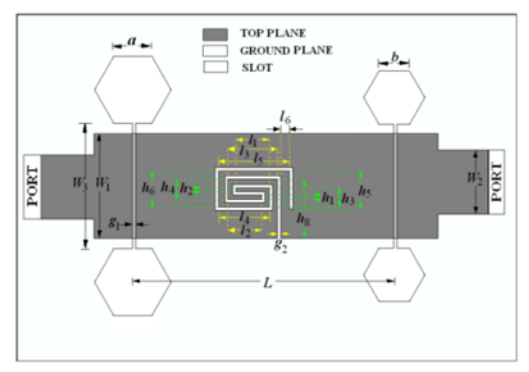


FIGURE 12. Schematic diagram of the proposed filter unit consists of spiral shaped defected slot at the signal plane and a hexagonal head dumbbell shaped defects in the ground plane.

A. SIMULATED RESULT OF THE COMBINED FILTER

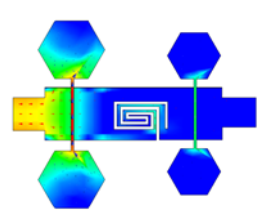
From the simulated S-parameters as shown in Fig.13, it is observed that the investigated filter shows a lowpass response. The investigated filter unit provides four transmission zeros at 3.2 GHz, 4.1 GHz, 4.9 GHz and 5.8 GHz with 3dB cutoff frequency at 3.1 GHz. The maximum insertion loss in the passband is 0.2 dB and sharpness 112.5dB/GHz. The 15dB rejection band is 3GHz.

Frequency(GHz)

FIGURE 13. Simulated S-parameter response of the proposed filter.

B. SURFACE CURRENT DISTRIBUTION OF THE COMBINED FILTER

The current distributions of the structure for the four transmission zeros are exhibited in Fig. 14 (a), (b), (c) and (d) respectively. It is clearly seen in Fig. 14 (a) and (d) that at the resonant frequencies f_{r1} = 3.2 GHz and f_{r4} = 5.8 GHz, there is high magnitude of surface current distribution around the spiral slot of the proposed defects on the microstrip structure. Hence it can be undoubtedly said that those resonant frequencies (f_{r1} = 3.2 GHz and f_{r4} = 5.8 GHz) are obtained by the proposed spiral defects on microstrip line. Among the rests, at the resonant frequency of f_{r2} = 4.1 GHz, there is a high magnetic current distribution in the slot of the bigger hexagonal head defects at ground and very less amount of current distribution present in the smaller defect. It is again observed in the S-parameter response that the rejection level at the pole frequency of 5 GHz is almost the same as that at resonant frequency of 4.1 GHz. This causes the bandwidth to be widened which is evident from the current distribution in Fig. 14(c).



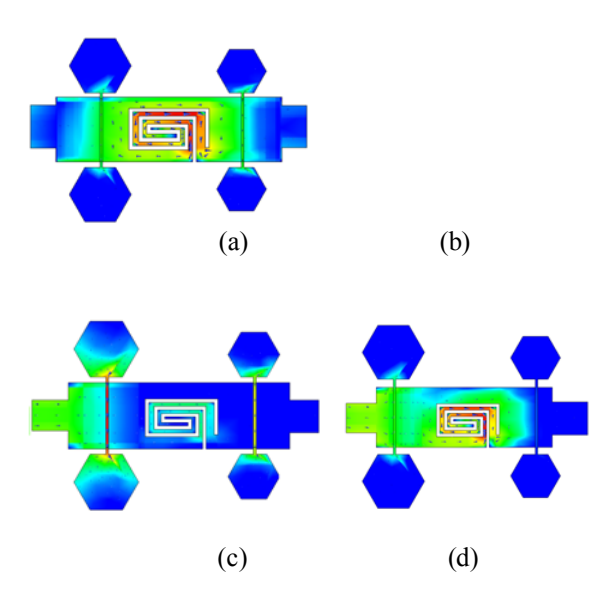
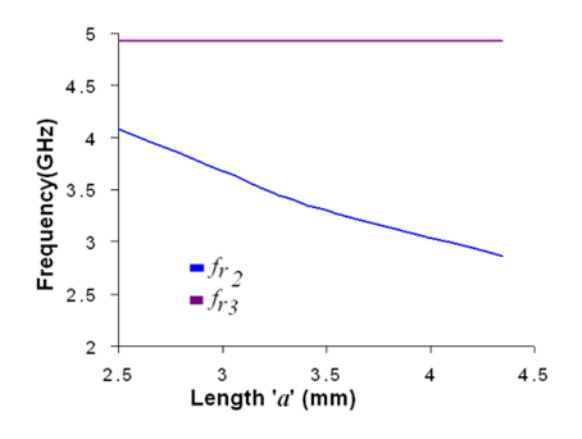


FIGURE 14. Layout of the surface current distribution of the proposed filter unit consists of spiral shaped defected slot at the signal plane and a hexagonal head dumbbell shaped defects in the ground plane for the frequencies (a) 3.2GHz, (b) 4.1GHz, (c) 5GHz and (d) 5.8GHz.

C. PARAMETRIC STUDY OF THE COMBINED FILTER

A parametric study is presented here to support the concept that the second and third resonant frequencies f_{r2} and f_{r3} are created due to the bigger and smaller hexagonal head dumbbell shaped defects. This parametric study is done which relates the dimension of the defected structures to the second and third resonant frequencies. From Fig. 15 (a) it is clearly seen that change in arm length (a) of bigger defects causes a significant change in second resonant frequency (f_{r2}) but causes no change in the third resonant frequency (f_{r3}) . Again it is observed in Fig. 15 (b) that variation in the arm length (b) of smaller defect causes a huge change in third resonant frequency (f_{r3}) but causes no change in the second resonant frequency (f_{r2}). Hence it can be concluded that the second resonant frequency is provided by bigger defect whereas the third resonant frequency is yielded by the smaller defect respectively.



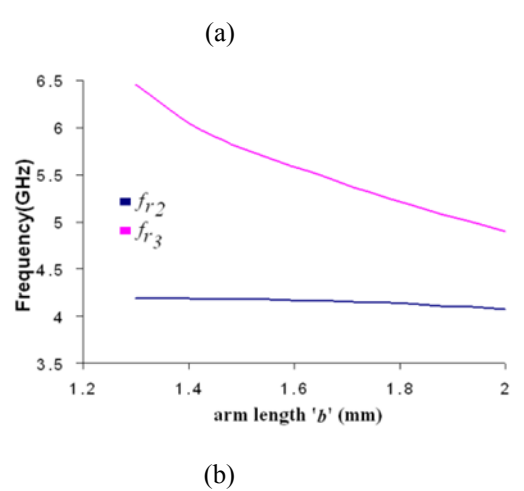


FIGURE 15. (a) variation of pole frequencies with the arm length 'a' of the hexagonal head of the bigger defects keeping the smaller defects dimension fixed, (b) variation of pole frequencies with the arm length 'b' of the hexagonal head of the smaller defect keeping the bigger defect dimension constant.

D. EQUIVALENT CIRCUIT OF THE COMBINED FILTER

For the proposed top and ground defects combined bandstop filter, the equivalent circuit shown in Fig. 16. The resonant frequencies of the filter are determined by the parallel resonant circuits, whose inductance and capacitance values are calculated from the equations (9 and 10) [23]. The first parallel resonant circuit is responsible for the lower pole frequency and the second one for the next higher pole frequency and so on. The cutoff frequencies are calculated by the series resonant circuits whose inductance and capacitance values are obtained by the equations (11 and 12) [23]. The first series resonant circuit determines the lower cutoff frequency of the proposed combined structure. The other series resonant circuit with the corresponding parallel resonant circuits establishes the bandwidth of the filter following the stagger tuning technique. The extracted values of the LC parameters are given as: L1=0.36nH, L2=0.48nH, L3=3.02nH, L4=3.61nHL5=16.08nHL7=1.17nH, C1=6.43pF, C2=3.09pF, C3=0.34pF, C4=0.2pF, C5=0.14pF, C6=0.13pF, C7=0.89pF, C=0.3pF. The comparison of the EM simulated and circuit simulated sparameter response is given in Fig. 17.

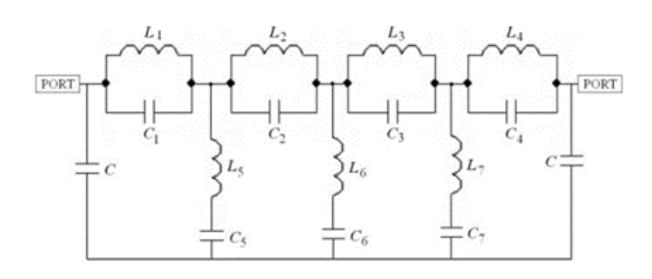


FIGURE 16. The equivalent circuit of the proposed DGS-DMS combined filter.

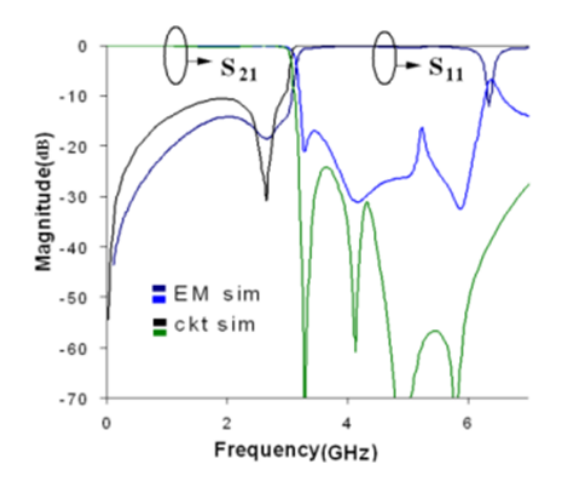


FIGURE 17. Comparison of EM simulated and circuit simulated responses.

$$C_1 = C_2 = \frac{f_c}{200\pi (f_0^2 - f_c^2)}$$
 (9)

$$L_1 = L_2 = \frac{1}{4\pi f_0^2 \mathcal{L}_1}$$
 (10)

$$C_2 = \left(\frac{\Omega_c FBW}{}\right) \frac{g}{}$$
(11)

$$L_2 = \frac{1}{\omega^2 C_2} \tag{12}$$

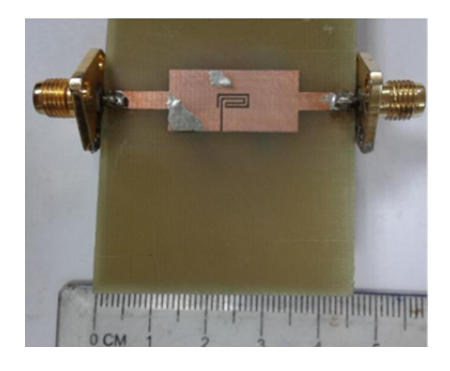
Where 'g' is the normalized source resistance or conductance, Ω_c is the normalized cutoff frequency and ω_0 =2 π f₀. The fractional bandwidth is given by equations (13) [24].

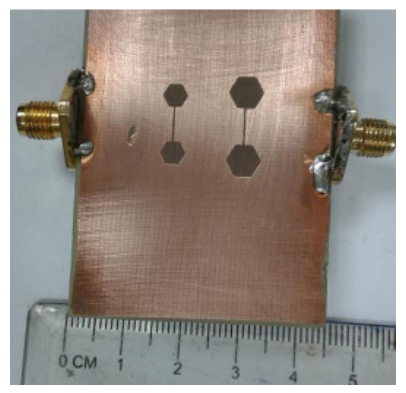
$$FBW = \frac{\omega_2 - \omega_1}{\omega_0}$$
 (13)

E. MEASURED RESULT OF THE COMBINED FILTER

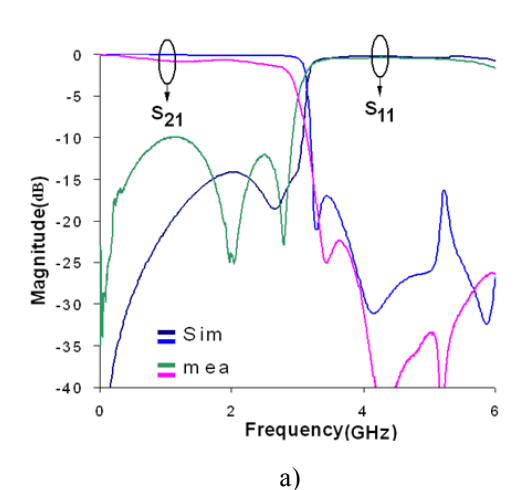
The filter is fabricated and the photographic view of the top plane and bottom plane of the filter is given in Fig. 18 (a) and (b) respectively. The measured s-parameter result is compared with the simulated one and illustrated in Fig. 19 (a). The simulated and measures phase response is given in Fig. 19 (b). The dissimilarity between simulated and measured S-parameter result may be due to the fabrication error. There is also a delay between simulated and measured response, which is because of the SMA connector length and could not be calibrated exactly.

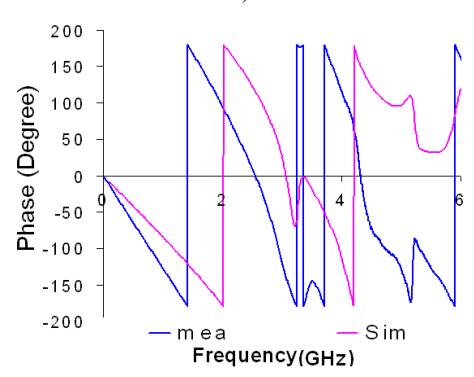
(a)





(b) FIGURE 18. Photograph of the structure of (a) top plane and (b) ground plane.





(b)

FIGURE 19. (a) Comparison of simulated and measured s-parameter results, (b) comparison of simulated and measured phase response.

IV. COMPARATIVE STUDIES

Fig. 20 shows a comparison of the transmission coefficients of top plane defect (DMS), ground plane defect (DGS) and combined defect (DGS-DMS). In this figure it is inevitable that combination of two bandstop filters provided by proposed spiral microstrip defect resonator and hexagon head DGS yields a lowpass filter with improved rejection band. The comparison study is also shown in terms of data in Table II. It is showing the different parameters of the individual filter responses of proposed spiral defect resonator and the hexagon head DGS separately along with the combination of the spiral defect resonator and the hexagon head DGS filter response. The following Table III shows the comparison of proposed filters with the existing literature available.

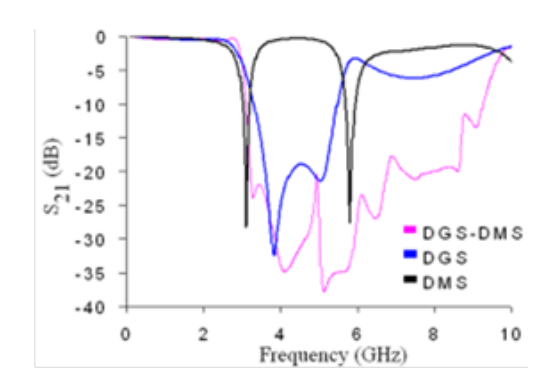


FIGURE 20. Comparison of simulated s-parameter results of spiral defect, hexagonal defect at round and combination of these to defects.

TABLE II. Comparison of Individual defects with proposed combined defects.

 NEL II. Companson of marviada derects with proposed combined derect					ou doloo
Defect type	f _c (GHz)	f _r (GHz)	FBW (%)	SF (dB/ GHz)	IL (dB)
Spiral	2.8-	3.1,	2.3,	55.6,76	0.3
defect	3.3,	5.8	1.7	.8	
	5.5-				
	6.3				
Hexagonal	2.9,	3.8,	39.08	33.4	0.5
head	5.8	5.03			
dumbbell					
shaped					
defects					
Combined	2.97,	3.3,4.	92.6	64.6	0.5
defects	9.68	4,5.1,			4
		6.3			

TABLE III.	Comparison of	of proposed	filter with	existing works.

Referenc es	Size (λ_g^2)	Sharpness factor (dB/GHz)	Stopb and (GHz	Rejec tion (dB)
[19]	0.005	19	8.58	-20
[20]	0.094	11.5	2	
[21]	0.005	60	1	-23
[22]	0.062	230.8	1.8	-20
proposed Filter combine d filter	0.065	112.5	3.83	-23

V. CONCLUSION

In this paper it can be clearly seen that using the combined spiral top plane defects & hexagonal head ground plane defects, the stop band width is increased from dual narrow band response to the wide band response of 4.2GHz with attenuation of -19dB. The proposed combined defect filter with improved stopband displays 92.6% FBW and 112.5 dB/GHz sharpness factor with very compact in size as 0.26 $\lambda_0 \times 0.25 \lambda_0$.

REFERENCES

- C. S. Kim, J.S. Park, D. Ahn and J.B. Lim, "A Novel 1-D Periodic Defected Ground Structure for Planar Circuits", IEEE Microw. Guided Wave Lett., vol. 10, No. 4, pp.131-133, Apr. 2000. DOI: 10.1109/75.846922.
- [2] D. Ahn, J. S. Park, C. S. Kim, J. Kim, Y. Qian, and T. Itoh, "A Design of the Low-pass Filter using the Novel Microstrip Defected Ground Structure," IEEE Trans. Microw. Theory Tech., vol. 49, no. 1, pp. 86–93, Jan. 2001. DOI: 10.1109/22.899965.
- [3] Y. Rao, H. J. Qian, B. Yang, G.-G. Roberto and X. Luo, "Dual-Band Bandpass Filter and Filtering Power Divider With Ultra-Wide Upper Stopband Using Hybrid Microstrip/DGS Dual-Resonance Cells," IEEE Access., vol. 8, pp. 23624–23637, Jan. 2020. DOI: 10.1109/ACCESS.2020.2970209.
- [4] R. S. Sangam, S. Dash and R. S. Kshetrimayum, "Ultra-Broadband Bandpass Filter Using Linearly Tapered Coupled-Microstrip Line and Open Loop Defected Ground Structure," IEEE Trans. on Circuit and System-II., vol. 68, no. 1, pp. 181–185, Jan. 2021. DOI: 10.1109/TCSII.2020.3009415.
- [5] J. Zhou, Y. Rao, D. Yang, H.-J Qian and X. Luo, "Compact Planar Tunable Filter With Constant Absolute Bandwidth and Wide-Frequency Tuning Range Using DGS Coupling Structure," IEEE Access., vol. 9, pp. 157259–157266, Dec. 2021. DOI: 10.1109/ACCESS.2021.3124218.
- [6] D. Tang, H.-J. Qian, Y. Dong and X. Luo, "Compact 1.75–2.7 GHz Tunable BPF With Wide Stopband Up to 9.5 GHz Using Harmonic-Controlled SIDGS Resonators," IEEE Trans. on Circuit and System-II., vol. 69,no. 11, pp. 4228–4232, Nov. 2022. DOI: 10.1109/TCSII.2022.3185805.
- [7] J. Wang, H. Ning, Q. Xiong and L. Mao, "A Compact Narrow-Band Bandstop Filter Using Spiral-Shaped Defected Microstrip Structure", Radioengineering, Vol. 23, No. 1, p-p. 209-213, 2014.
- [8] F. Wei, Y. Pei-Yuan Qin, J. Guo, and X. W. Shi, "Design of multiband bandpass filters based on stub loaded steppedimpedance resonator with defected microstrip structure," IET Microw. Anten. Propag., vol. 10, no. 2, pp. 230–236, Jan., 2016. DOI: 10.1049/iet-map.2015.0495.
- [9] L. Chen, X.-Y. Li and F. Wei, "A Compact Quad-Band Bandpass Filter Based on Defected Microstrip Structure",

- Frequenz, Vol.71, no.7-8, p-p. 311-316, Feb., 2017. DOI: 10.1515/freq-2016-0238.
- [10] X. Zheng, Y. Pan and T. Jiang, "UWB Bandpass Filter with Dual Notched Bands Using T-Shaped Resonator and L-Shaped Defected Microstrip Structure", *Micromachines*, Vol.9, no.6, pp. 1-11, Jun., 2018. DOI: 10.3390/mi9060280.
- [11] S. G. Mehraban, N. Masoumi and S.-N. Safieddin, "A quasianalytic synthesis methodology for spiral defected microstrip compact bandstop filters", *International Journal of RF & Microwave Computer-Aided Engg.*, Vol.30, no.12, p-p. 1-11, Dec., 2020. DOI: 10.1002/mmce.22467.
- [12] S. Shakeri, M. Dousti and B. Ghalamkari, "A quad-band defected microstrip structure loaded bandpass filter for standard GPS, WiFi, WLAN, and WiMAX applications", *International Journal of RF & Microwave Computer-Aided Engg.*, Vol.32, no.5, p-p. 1-11, Jan., 2022. DOI: 10.1002/mmce.23082.
- [13] Y.-N. Han, Z.-H. Liu, C.-Y Cheng, and Y.-Y. Zhou, "Dual-Band Bandstop Filtering Cable Design Using Defected Conductor Layer With Asymmetric Spiral Structure", *IEEE Trans. Microw. Theory Tech.*, Vol.70, no.6, p-p. 3154-3162, 2022. DOI: 10.1109/TMTT.2022.3157855.
- [14] A. Tirado-Mendez, H. Jardon-Aguilar, and R. Flores-Leal, "Improving Frequency Response of Microstrip Filters using Defected Ground and Defected Microstrip Structures", Progress In Electromagnetics Research, Vol. 13, p-p. 77–90, 2010. DOI: 10.2528/PIERC10011505.
- [15] A. Boutejdar, A. Omar, M. Al Sharkawy and A. Darwish, "A Simple Transformation of Improved WLAN Band Pass to Low Pass Filter Using Defected Ground Structure (DGS), Defected Microstrip Structure (DMS) and Multilayer-Technique", Journal of Microwaves, Optoelectronics and Electromagnetic Applications, Vol. 12, No. 1,p-p.111- 130, June 2013. DOI: 10.1590/S2179-10742013000100010.
- [16] J. Wang, H. Ning, Q. Xiong, M. Li and L. Mao, "A Novel Miniaturized Dual-band Bandstop Filter Using Dual-plane Defected Structures", Progress In Electromagnetics Research, Vol. 134, p-p. 397–417, 2013.
- [17] A. Boutejdar, A. Omar and E. Burte, "High-performance Wide Stop Band Low-pass Filter Using A Vertically Coupled DGS-DMS-Resonators and Interdigital Capacitor", Microwave And Optical Technology Letters, Vol. 56, No. 1, p-p. 87-90, January 2014. DOI: 10.1002/mop.28031.
- [18] S. M. Meeper, A. H. Hussein and M.A. Attia, "Design of a Novel Ultrawide Stopband Lowpass Filter Using a DMS-DGS Technique for Radar Applications", *Journal of Engineering Research*, Vol. 2, p-p. 128–130, 2015. DOI: 10.1155/2015/101602.
- [19] A. Boutejdar, M. Challal, S. Das and E. H. Soumia, "Design and Manufacturing of a Novel Compact 2.4 GHz LPF Using a DGS-DMS Combination and Quasi Octagonal Resonators for Radar and GPS Applications", Progress In Electromagnetics Research C, Vol. 90, p-p. 15–28, 2019. DOI: 10.2528/PIERC18092107.
- [20] B. Priya Annadurai and U. Hyder Ali, "A compact SIW bandpass filter using DMS-DGS structures for Ku-band applications", Sadhana, Journal of the Indian Academy of Sciences, Spinger, Vol.45, no.1, p-p. 1-5, 2020. DOI: 10.1007/s12046-020-01485-0.
- [21] B. Dokmetas, G.-O. Arican, N. Akcam and E. Yazgan, "A Compact Bandstop Filter Design Using DMS-DGS Technique for Radar Applications", Applied Computational Electromagnetics Society Journal (ACES), Vol.36, no.11, p-p. 1460-1467, Nov. 2021.
- [22] L. Liu, H. Fan, R. Jin, X. Bai and J. Geng, "Compact Wideband Bandstop Filter With Directly Controlled Rejection", *IEEE* Transactions on Circuits and Systems II, Vol.68, no.7, p-p. 2282-2286, 2021. DOI: 10.1109/TCSII.2021.3049693.
- [23] C.-W. Tang and C.-H. Yang "New Method for the Microstrip Bandstop Filter with a Wide Stopband and an Extremely High Attenuation", *IEEE* Transactions on Circuits and Systems II, Vol.69, no.11, p-p. 4318-4322, 2022. DOI: 10.1109/TCSII.2022.3179300.



[24] J.S. Hong and M.L. Lancaster, "Microstrip Filters for RF/Microwave Applications", New York: Willy, 2001.